ADVANCED FUNCTIONAL MATERIALS
www.afm-journal.de

Materials Views
www.MaterialsViews.com

Systematic Control of Nucleation Density in Poly(3-Hexylthiophene) Thin Films

Edward J. W. Crossland, Khosrow Rahimi, Günter Reiter, Ullrich Steiner, and Sabine Ludwigs**

While molecular ordering via crystallization is responsible for many of the impressive optoelectronic properties of thin-film semiconducting polymer devices, crystalline morphology and its crucial influence on performance remains poorly controlled and is usually studied as a passive result of the conditions imposed by film deposition parameters. A method for systematic control over crystalline morphology in conjugated polymer thin films by very precise control of nucleation density and crystal growth conditions is presented. A precast poly(3-hexylthiophene) film is first swollen into a solution-like state in well-defined vapor pressures of a good solvent, while the physical state of the polymer chains is monitored using in situ UV–vis spectroscopy and ellipsometry. Nucleation density is selected by a controlled deswelling of the film or by a self-seeding approach using undissolved crystalline aggregates that remain in the swollen film. Nucleation densities ranging successively over many orders of magnitude are achieved, extending into the regime of spherulitic domains 10 to 100 μm in diameter, a length scale highly relevant for typical probes of macroscopic charge transport such as field-effect transistors. This method is presented as a tool for future systematic study of the structure-function relation in semicrystalline semiconducting polymers in a broad range of applications.

1. Introduction

The great promise of semiconducting polymers in organic electronic devices stems from the combination of low-cost solution processing with interesting optoelectronic properties such as high charge transport mobility. Many of the best performing conjugated polymers, including the poly(alkylthiophene)s, derive their high charge mobility from an ability to crystallize.[1,2] While charge transport along an individual conjugated chain is predicted to be extremely rapid,[3] over longer distances charge must also pass between chains.[4] Crystallization aids interchain charge transfer by bringing planarized chains together in regular, more intimate contact. The importance of crystalline morphology has been established by previous studies reporting the sensitivity of measured charge transport to film formation parameters that impose the kinetics of crystallization.[5–7] However, systematic study of transport-limiting morphological features and how one might optimize crystalline structure remain extremely challenging because of the difficulty of incremental control over crystallization. In particular, typical solution casting conditions (even from high boiling point carrier solvents[5]) lead to extremely high nucleation density, such that macroscopic charge transport probes average over an enormous number of randomly oriented grain boundaries whose density is neither well-known or easily adjusted.[8,9] Methodologies, such as self seeding, adapted from studies of classical semicrystalline polymers, exist that permit systematic control of important morphological characteristics such as nucleation density and lamellar width. We show how controlled solvent swelling and deswelling of a precast poly(3-hexylthiophene) (P3HT) film is an extremely effective method for controlling crystalline morphology (independent of film formation) by fully incremental control of nucleation density over many orders of magnitude.

In P3HT and many other main chain conjugated polymers, crystallization is dominated by strong π–π interactions perpendicular to the thiophene ring, which drive a highly anisotropic growth of stacked aggregates. When confined to a thin film, the π-stacking [010] direction lies in-plane, with the molecules adopting an edge-on orientation ([100] alkyl side chains aligned perpendicular to the substrate). Long crystalline lamellae separated by amorphous regions containing chain folds and ends provide efficient in-plane transport channels along the π-stacking direction. Device transport characteristics,

---

Dr. E. J. W. Crossland, Prof. U. Steiner, Dr. S. Ludwigs
Freiburg Institute for Advanced Studies (FRIAS)
University of Freiburg
Albert-Str. 19, 79104 Freiburg, Germany
E-mail: edward.crossland@frias.uni-freiburg.de;
sabine.ludwigs@makro.uni-freiburg.de

K. Rahimi, Prof. G. Reiter
Physikalisches Institut
University of Freiburg
Hermann-Herder-Str 3a, 79104 Freiburg, Germany

Prof. U. Steiner
Cavendish Laboratory
J. J. Thomson Avenue
University of Cambridge
Cambridge CB3 0HE, UK

Dr. S. Ludwigs
Freiburg Materials Research Center and Institute for Macromolecular Chemistry
University of Freiburg
Stefan-Meier-Str. 21, 79104 Freiburg, Germany

DOI: 10.1002/adfm.201001682

determined by the slowest transfer processes, are dominated by passage of charge from one ordered domain to another, traversing crystalline-amorphous interfaces and domain boundaries.[9,10] We can therefore identify two key morphological scales which determine transport properties: i) The degree of intrachain macromolecular order and the strength of π–π interactions and ii) the mesoscale morphology comprising the size and relative orientation of microcrystalline domains separated by less-ordered and amorphous zones.[11,12] Both of these morphological scales can be effectively addressed by both molecular design (M_W, side chain chemistry, regularity, and density[13–15]) and by crystallization kinetics.

Previous investigations studying the impact of film processing on measured charge mobility in a semicrystalline polymer film have compared, for example, films cast from different carrier solvents[5–7] or using coating methods such as spin or dip coating and drop casting.[1,16–18] Broadly speaking, an inverse correlation is observed between the rate of solvent removal, that is the time allowed for self organization, and the resulting charge mobility.[5,19] However, comparison of these relatively uncontrolled processing conditions leads to a convolution of effects caused by changes in both local intrachain order and the frequency of domain boundaries. Nucleation density determines the number of domain boundaries, while local intrachain order is affected by the growth rate since this determines the time available for each chain to rearrange at the growth front. Independent and incremental control of these parameters will allow informed optimization of semicrystalline polymer devices, which is of particular importance for the screening of potentially high-performing polymer materials whose crystalline morphology happens not to be optimized by crystallization conditions imposed by standard film casting.

Two rather simple approaches exist to change nucleation density in a polymer solution. Firstly one can increase the degree of supercooling by lowering the temperature or increasing the concentration, in effect, the continuous process in a drying polymer film. A much more controlled approach, however, is to decouple crystallization from film formation by melting and recrystallizing a preformed film under well-defined isothermal conditions. A second possibility is to seed crystallization with a known density of nucleii. One such method, self seeding, relies on a property unique to polymer crystals, i.e., the simultaneous presence of many kinetically trapped metastable states, each with a different melting temperature.[20,21] Again starting from a preformed, precrystallized film, the aim is to first melt all but the thermodynamically most stable crystals, which then act as nucleation centers (seed crystals) under subsequent recrystallization conditions. Because the nucleation barrier is removed, crystallization can be induced under very low degrees of supercooling (slow growth) where one would normally have to wait a prohibitively long time for nucleation. This concept also provides an independent handle on nucleation density under fixed crystallization conditions (i.e., constant growth rate). The application of these ideas to semiconducting polymer films using thermal treatment of the melt state is not ideal since elevated temperatures tend to degrade conjugated polymers and high melt viscosity means that unreasonably long times are required for crystal growth at the relatively low degrees of supercooling necessary to achieve low nucleation densities. Low nucleation densities are of interest because charge transport measurements typically probe length scales of several micrometers or more and average over an enormous number of grain boundaries.[8] Measurements within individual grains and across isolated boundaries are therefore extremely difficult.

As an alternative, an approach based on controlled solvent swelling and deswelling of a preformed P3HT film in well-defined vapor pressures of a good solvent is presented. In situ ellipsometry and UV-vis absorbance spectroscopy show that at high enough degrees of swelling, all detectable traces of the crystal phase disappear, while the film remains a uniform thin layer covering the substrate. A concentrated solution of isolated P3HT chains in a flexible coil configuration with an effective concentration that can be adjusted at will by changing the solvent vapor pressure is thus produced. All memory of the crystalline morphology present after film formation can be erased. Recrystallization is induced under very precise conditions by deswelling the layer to form a supersaturated solution and allows direct, in situ observation of the nucleation and growth process in the film using polarized optical microscopy. The successful application of this controlled crystallization method to P3HT films offers several significant advantages. Firstly, nucleation density can be reduced significantly below that typically observed after spin-coating or drop casting, such that domain sizes reach the scale of typical macroscopic charge transport probes (tens of micrometers) in a technologically relevant, uniform thin-film geometry. Micrometer scale spherulitic structures were reported by Lu et al. after exposing poly(3-butylthiophene) films to fixed vapor pressures of carbon disulfide (CS_2) for many hours, however in this case the low nucleation density was reported to be caused by nucleation and growth of a more stable polymorph.[22,23] More importantly, self seeding allows incremental control of the nucleation density independent of growth rate. These results confirm that P3HT crystallization in thin films follows the expected physics of nucleation and growth for a semicrystalline polymer. This technique provides an ideal platform for study of the structure-function relationship for charge transport in semicrystalline semiconducting polymers.

2. Results and Discussion

A P3HT film (thickness d_0) spin-coated from 1,2,4-trichlorobenzene was used as the starting state for all solvent swelling experiments. A controlled solvent vapor pressure was achieved by mixing two streams of dry nitrogen carrier gas, one of which was first saturated by bubbling through a wash bottle containing the chosen solvent. The mixing ratio, and therefore relative vapor pressure (hereafter denoted as $P_{vap} = P/P_{sat}$, where P denotes the actual vapor pressure and P_{sat} denotes the saturated vapor pressure), was controlled using two mass flow controllers (MKS Instruments, Munich, Germany) with an accuracy of 0.01 sccm (standard cubic centimeters per minute) in a total flow of 20 sccm. The temperature of the solvent reservoir and chamber was fixed at 21.0 °C using a water thermostat that also circulated through the chamber walls. The sample temperature was set independently to 19.0 °C on a Peltier stage mounted in the base of the chamber. A schematic of the chamber used for in situ optical characterization of the polymer film during swelling is shown in the Supporting Information. When exposed to the vapor of a good solvent, in this case CS_2, the film swells in thickness and the volume fraction of polymer (Φ_p) correspondingly decreases. The ratio of the ellipsometrically determined swollen film thickness (d) to the starting thickness (d_0) can be used to approximate Φ_p at any solvent vapor pressure, as shown in **Figure 1**a. Two swelling regimes are visible as P_{vap} is increased stepwise from 10 to 90% of saturation (with 300 s equilibration time at each P_{vap}). Moderate swelling up to approximately 81% is followed by a rapid decrease in Φ_p such that at 90% of the saturated vapor pressure, the polymer concentration in the layer is just 13%.

The physical conformation of the polymer chains can be inferred from the optical absorbance of the film as the solvent content in the layer increases. The absorption spectrum, shown in Figure 1b, can be interpreted as a simple coexistence of two distinct populations of different molecular states, according to the model of Spano et al.[24] The long wavelength absorbance comprising distinct vibronic peaks is attributable to chains in the crystalline state, that is, linearized π-stacked chains forming weakly interacting H-aggregates. The second population contributes a single broad absorption peak at short wavelength (465 nm) arising from intrachain states of isolated chains in a flexible coil conformation.[25]

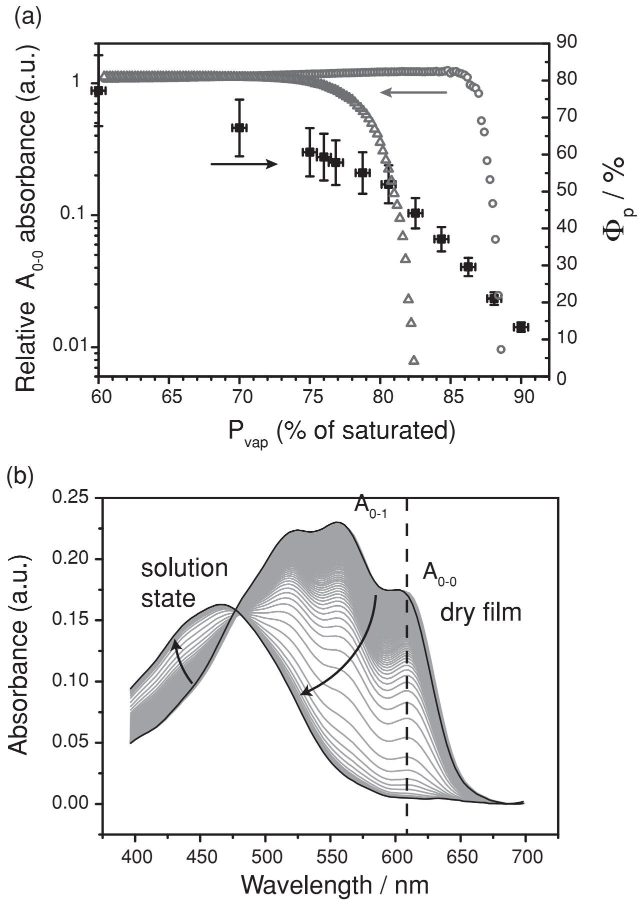

Figure 1. Controlled dissolution and recrystallization of P3HT thin films in CS_2 solvent vapor. a) Polymer concentration ($\Phi_p = d_0/d$) in the solvent-swollen film from ellipsometric calculation of film thickness (■). The initial thickness was d_0 = 40 nm. The A_{0-0} (610 nm) crystalline phase absorption relative to the initial dry film is shown during swelling (○) and deswelling (Δ) at 0.2% min^{-1}. b) Full UV-vis absorbance spectra for the film in (a) swollen to 90% P_{vap}.

The spectrum of the initial dry film is dominated by the long wavelength aggregate absorption, with clear A_{0-1} and A_{0-0} (where subscripts denote respective vibronic transitions) peaks at 555 nm and 610 nm, respectively. As P_{vap} increases, the intensity of the aggregate absorbance diminishes while the low wavelength absorption grows correspondingly, with an isosbestic point visible at 479 nm. This transition marks the dissolution of crystalline regions with increasing solvent content and is conveniently tracked in situ by monitoring the strength of the A_{0-0} absorption (where the amorphous phase does not absorb) as a function of P_{vap} (Figure 1a). The transition begins around 84% P_{vap}, shortly following the onset of increased swelling seen in ellipsometry (Figure 1a). Above this point there is a coexistence of crystalline aggregates and dissolved chains. The A_{0-0} absorbance continues to fall until, at 88.6% P_{vap}, the signal reaches the detection limit of the spectrometer. The film is then swollen to such an extent that a uniform 300-nm-thick liquid film, in which the vast majority of polymer chains adopt an isolated coil-like configuration, is obtained.

Thus prepared, this thin-film solution represents a very useful starting state since it can be used to induce recrystallization under well-defined conditions (polymer concentrations) by reducing P_{vap} to deswell the film. Drying the film rather slowly (0.2% min^{-1}), the A_{0-0} peak reappears at 82% P_{vap}, signifying recrystallization in the supersaturated solution. There is, as expected, a sizeable hysteresis in the onset of this peak since a significant quench is needed for the nucleation and growth of the crystalline phase within reasonable waiting times.

A 40-nm P3HT film viewed after spin-coating shows very weak or no optical birefringence when viewed between crossed polarizers because of the very high nucleation density that results from rapid and uncontrolled crystallization (see Supporting Information). At a length scale of micrometers and above, the in-plane molecular orientation is isotropic. In our case, however, the nucleation density can be significantly reduced by choosing a Φ_p only slightly above some critical concentration (Φ_0), such that it becomes possible to observe the nucleation and growth of P3HT crystallites in real time using polarized optical microscopy (POM). **Figure 2**a shows typical POM images taken of films after 1800 s crystallization at a series of decreasing solvent vapor pressures (P_{vap}^{cryst}) after initial swelling (P_{vap}^{intial}) for 600 s at 91% (well above the disappearance of spectroscopic traces of polymer aggregates at 88.6% $P_{vap}^{initial}$). After recrystallization a well-developed spherulitic morphology with a characteristic Maltese cross pattern is seen in which bright regions indicate a common in-plane alignment of the P3HT molecule (optic axis) oriented at 45° to the polarizers. The molecular interpretation of this morphology is discussed further below. The number density of spherulites, summarized in Figure 2b, is a direct measure of nucleation density and is strongly dependent on P_{vap}^{cryst}. Indeed, the nucleation density decreases by an order of magnitude between P_{vap}^{cryst} of 76.0 and 81.0%.

To gain further insight into the degree of local intrachain order following crystallization we refer again to the H-aggregate model of Spano et al. Using the UV-vis spectra in Figure 2c, the

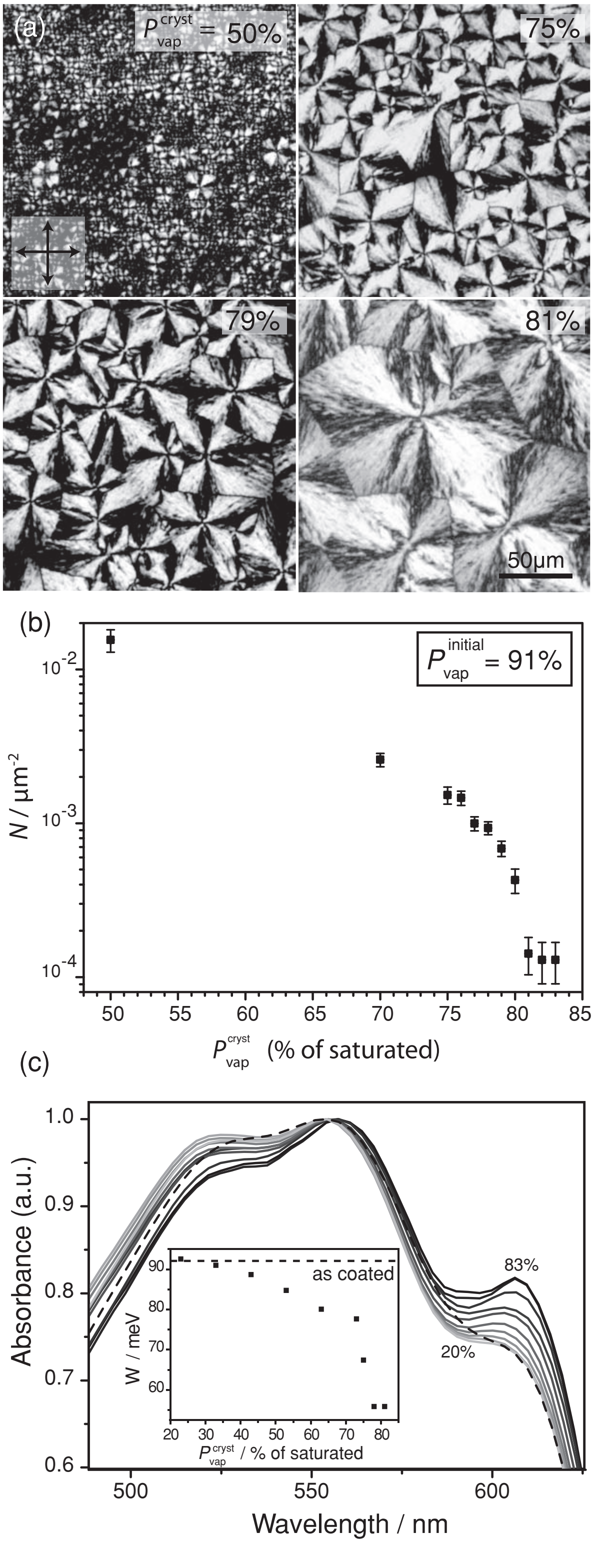

Figure 2. P3HT nucleation density. a) POM images (200 µm × 200 µm) of a 40-nm-thick P3HT film crystallized for 1800 s at the stated P_{vap}^{cryst} after initial swelling at 91.0% $P_{vap}^{initial}$ for 600 s. b) Nucleation density as a function of P_{vap}^{cryst} from the POM images. c) Normalized UV-vis spectra of dry P3HT films as spin-coated from 1,2,4-trichlorobenzene (dashed) or crystallized in controlled CS_2 solvent vapor at P_{vap}^{cryst} ranging from 20 to 83% (crystallized for 2000 s, followed by drying at 2% min^{-1}).

free exciton bandwidth within the crystalline phase (W) can be calculated from the intensity ratio (A) of the A_{0-0} to A_{0-1} absorbance bands according to:[24]

$$A = \frac{A_{0-0}}{A_{0-1}} = \left(\frac{1 - 0.24W/E_p}{1 + 0.73W/E_p}\right)^2 \tag{1}$$

where E_p is the energy of the main intramolecular transition (assumed to be 0.18 eV corresponding to a symmetric C=C stretch). According to Clark et al.[19] a decrease in W (manifested in the spectra as an increase in A), assuming similar interchain order, would be consistent with an increase in the effective conjugation length (more linearized, better ordered polymer chains). Figure 2c (inset) shows the extracted W values of dry films following crystallization at the stated P_{vap}^{cryst} alongside that of the starting spin-coated film. The exciton bandwidth decreases with increasing P_{vap}^{cryst}, which is associated with the slower crystallization kinetics under incrementally lower degrees of undercooling.

Returning to the nucleation density of Figure 2b, the nucleation density is found to reach a plateau at 82% and 83% as the degree of undercooling is reduced. Relying solely on homogeneous nucleation, one would expect to find a threshold concentration below which no nucleation events occur on the experimental timescale. The anomalously high, and constant, nucleation observed at 82% and 83% suggests the presence of additional nucleation centers in the initially swollen film that are able to grow above 81% P_{vap}^{cryst}, even in the absence of new homogeneous nucleation. A potential source of such nucleation centers is the polymer crystals themselves, that is, microscopic polymer aggregates that remain undissolved by the initial swelling procedure even after the disappearance of spectroscopically visible aggregates. To investigate the possibility of self-seeding we repeated crystallization at very low supercooling (83% P_{vap}^{cryst} for 1800 s), but after varying the degrees of swelling of the initial film (**Figure 3** inset). If only the most

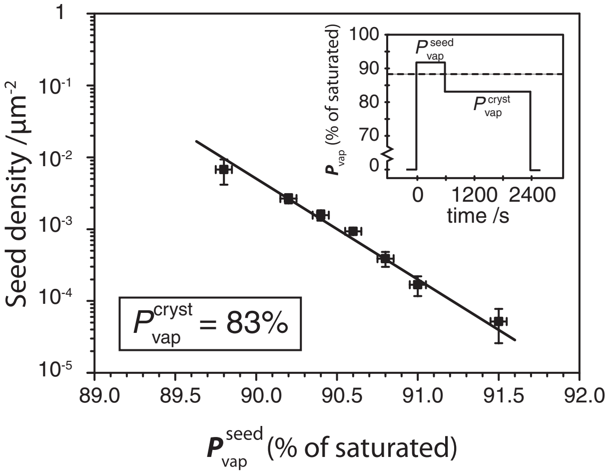

Figure 3. Self-seeding density remaining in the swollen P3HT film as a function of P_{vap}^{seed}, inferred from counting the nucleation density after recrystallization at 83% P_{vap}^{cryst}. Inset: applied P_{vap} protocol showing the initial seeding stage (P_{vap}^{seed}) followed by crystallization at fixed P_{vap}^{cryst} (dashed line indicates spectroscopically determined dissolution of crystalline regions in the initial film). No nucleation was observed at 83% P_{vap}^{cryst} following seeding at 93% P_{vap}^{seed}.

thermodynamically stable polymer crystals remain undissolved at P_{initial} (hereafter denoted as $P_{\mathrm{vap}}^{\mathrm{seed}}$), the number density of surviving seed nucleii is expected to depend on the degree of initial swelling. By counting the number density of spherulites that grow at 83% $P_{\mathrm{vap}}^{\mathrm{cryst}}$ the density of self-seeding nucleii present in the initially swollen film could be inferred. The results of this experiment are shown in Figure 3 (POM images are included in Supporting Information). It was found that the nucleation density at 83% $P_{\mathrm{vap}}^{\mathrm{cryst}}$ decreases exponentially with increasing $P_{\mathrm{vap}}^{\mathrm{seed}}$. No spherulites were observed after initial swelling to 93% $P_{\mathrm{vap}}^{\mathrm{seed}}$, which implies that no homogenous nucleation occurs at 83% $P_{\mathrm{vap}}^{\mathrm{cryst}}$ on the experimental timescale, such that all crystallites grow from seed nucleii. The exponential fall in seed density is similar to that reported by Xu et al. with increasing temperature in a crystallizable block copolymer and organometallic homopolymer.[21]

A great attraction of self seeding is the ability to change nucleation density over orders of magnitude, while maintaining otherwise identical crystallization conditions. To demonstrate this effect a fixed 75.0% $P_{\mathrm{vap}}^{\mathrm{cryst}}$ that led to rather complete crystallization was chosen and only the starting seed density was changed through control of $P_{\mathrm{vap}}^{\mathrm{seed}}$. **Figure 4**a,d compares the POM morphology of films with high and low extremes of seed density at $P_{\mathrm{vap}}^{\mathrm{seed}}$ of 91% or 88.6% and subsequently crystallized for 1800 s at 75.0% $P_{\mathrm{vap}}^{\mathrm{cryst}}$. The film with low seed density (91% $P_{\mathrm{vap}}^{\mathrm{seed}}$) shows clear spherulitic structures with an average diameter of 31 μm. Nucleation under these conditions is dominated by homogeneous nucleation (at 91% $P_{\mathrm{vap}}^{\mathrm{seed}}$ the seed density is 1.7 per 10^4 μm^2 compared to the final nucleation density of 15 per 10^4 μm^2). In contrast, only very weak background texture is visible in a POM image of the film seeded at 88.6% $P_{\mathrm{vap}}^{\mathrm{seed}}$ (Figure 4d brightness and contrast are enhanced here for clarity), which is consistent with an extremely high nucleation density. Tapping mode atomic force microscopy (AFM) (Figure 4b,c,e,f) reveals the origin of the POM morphologies at the scale of the crystalline lamellae. In all cases the charateristic edge-on crystalline lamellae with spacing 30 nm ± 4 nm is observed. Wide-angle grazing incidence X-ray and transmission electron microscopy (TEM) diffraction (included in the Supporting Information) are consistent with the often-observed edge-on orientation of the P3HT chains ([100] alkyl chain direction parallel to the substrate normal) both after spin-coating and after recrystallization from CS_2. We conclude therefore that the P3HT chains span the width of the lamellae, while the long direction arises from [010] π-stacking. The lamellae within each spherulitic domain of the low nucleation density film show a clear cooperative common orientation, which gives rise to the bright and dark regions in POM images. Because of the much higher nucleation density in the 88.6% $P_{\mathrm{vap}}^{\mathrm{seed}}$ seeded sample, we find that the crystalline lamellae are essentially without common orientation at the micrometer scale and above. Both films were however crystallized under identical conditions from a swollen state with no detectable spectroscopic trace of remaining P3HT crystallites. We stress that the nucleation density can be changed incrementally between these two extremes using this self-seeding approach.

The influence of crystallization conditions on intrachain order was further studied by comparing the long spacing of crystalline lamellae (obtained by fast Fourier transform (FFT) of tapping mode AFM images) as a function of $P_{\mathrm{vap}}^{\mathrm{cryst}}$

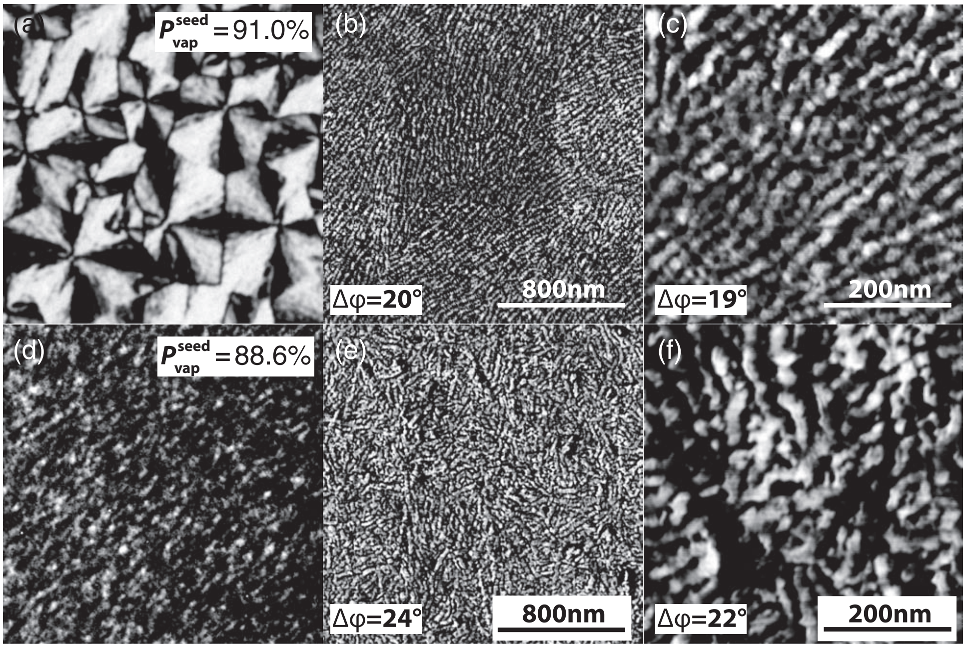

Figure 4. POM and AFM images of P3HT crystal morphology after crystallization at 75% $P_{\mathrm{vap}}^{\mathrm{cryst}}$ from low and high self seed densities. a) POM image (100 μm × 100 μm) of a low seed density film (91.0% $P_{\mathrm{vap}}^{\mathrm{seed}}$) alongside low (b) and high (c) magnification tapping mode AFM phase images showing common alignment of crystalline lamellae within the bright domains visible in POM. d–f) Equivalent images for a high seed density crystallization (88.6% $P_{\mathrm{vap}}^{\mathrm{seed}}$) reveal an essentially isotropic orientation of crystalline lamellae at the micrometer scale. AFM phase scale ($\Delta\phi$) is indicated for each image.

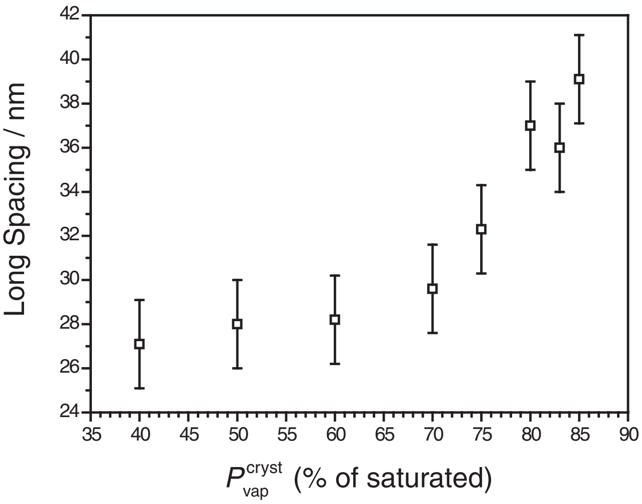

Figure 5. Lamellar long spacing as a function of $P_{\rm cryst}$ extracted by FFT of tapping mode AFM (phase) images. Films were crystallized for 2000 s at $P_{\rm vap}^{\rm cryst}$ (91% $P_{\rm vap}^{\rm seed}$) before drying at 2% min^{-1}. Crystallization at 85% was seeded at 89.0% $P_{\rm vap}^{\rm seed}$ for 300 s then held at $P_{\rm vap}^{\rm cryst}$ for 20 h before drying at 0.13% min^{-1}.

(**Figure 5**). The increase in long spacing is consistent with the trend towards increased intrachain order implied by the UV-vis spectra of Figure 2c. Within a given solvent–polymer system, the degree of local order characterized both by exciton bandwidth and the lamellar long spacing increases as crystallization kinetics slow (higher $P_{\rm vap}^{\rm cryst}$).

3. Conclusions

In summary, we have demonstrated a general method for extremely fine control over crystalline morphology in crystallizable semiconducting polymer films based on swelling and deswelling of preformed films in controlled solvent vapors. Nucleation density can be chosen at will by controlling the degree of supercooling in the swollen film during crystallization (homogeneous nulceation) or by self seeding the film by deliberately incomplete dissolution of polymer crystallites present in the initial spin-coated film. Self seeding has the significant advantage of permitting incremental changes in the nucleation density over orders of magnitude under otherwise identical crystal growth conditions. Additionally, crystallization can be extended to low concentrations where homogeneous nucleation is not observed and where crystallization kinetics are very slow. Improved intrachain order observed under slow crystallization kinetics is expected to be beneficial for charge transport properties within domains. Controlling nucleation density using this method provides very sensitive control of the spontaneous cooperative assembly of the crystalline lamellae over distances of many tens of micrometers, requires no complicated external triggers or applied fields, and is not tied to film coating conditions. Large-scale spherulitic morphologies provide an ideal system to investigate the structure-function relationship in semicrystalline polymer semiconductors. In particular we will be able to probe the importance of isolated domain boundaries in determining in-plane charge transport. These studies are currently being undertaken and will be the subject of a future report.

4. Experimental Section

Film preparation: Silicon (p-doped, Si Materials, Landsberg, Germany) and glass substrates were first cleaned in a CO_2 snow jet followed by exposure to oxygen plasma (Femto 100 W, Diener electronic, Gemany) for 300 s. P3HT was obtained from Merck Chemicals (Germany, M_n = 30.9 kg mol^{-1} from gel permeation chromatography (GPC), polydispersity index (PDI) = 1.9, 96.2% regioregular, estimated contour length from M_n 40–70 nm[12,26]) and BASF (Germany, Sepiolid P200, M_n = 31.9 kg mol^{-1}, PDI = 2.36, 98% regioregular). The polymer was purified in a two step procedure to eliminate bromine end groups and to remove catalyst residues. Firstly, an excess of nBuLi was added to an anhydrous toluene solution at room temperature and the mixture stirred and heated to 60 °C for 30 min. The polymer was precipitated in methanol. Catalyst residues were removed by vigorously stirring a P3HT solution in toluene with a 1 M solution of EDTA sodium salt in water for 1 h. The organic phase was extracted and dried over magnesium sulfate and passed through a short silica column before final precipitation in methanol to obtain the purified polymer. All nucleation density and AFM results reported here are for P3HT from Merck. Results from Rieke P3HT were qualitatively identical but produced marginally less well-defined spherulitic morphologies after crystallization from the initially swollen film. Thin films were spin coated from 20 mg mL^{-1} solutions in 1,2,4-trichlorobenzene (TCB) at 4000 rpm. The films were dried under N_2 for 10 min at 85 °C to remove residual solvent. All polymer solutions and films were prepared in a dry nitrogen atmosphere.

Ellipsometry and UV–vis spectroscopy: Ellipsometric measurements were made on Rieke P3HT films using a Nanofilm EP3-SE imaging nulling ellipsometer (Accurion, Goettingen, Germany) with 833.4 nm illumination, where the absorption in P3HT is negligible. The dry film was first characterized by fitting the ellipsometric parameters for a range of incident angles between 66° and 76° (from vertical). A best-fit refractive index of 1.86 and a thickness of 41 nm were found (in good agreement with thickness measured by X-ray reflectometry (38 nm) and AFM stepheight (40 nm)). Ellipsometric studies in well-defined vapor atmospheres were made in a chamber with quartz glass windows fixed perpendicular to the 60° incident and detection directions. The film was allowed to equilibrate for 300 s at each chosen solvent vapor pressure before each measurement. Fitted film thicknesses were highly consistent in repeated swelling experiments (within ca. 2 nm at a low degree of swelling and ca. 5 nm above 80% $P_{\rm vap}$). UV-vis absorption spectra were taken in a reflection geometry, with the film on a glass substrate coated on the reverse side with a 100-nm-thick thermally evaporated aluminium mirror. A single bifurcated optic fiber mounted at 90° above the chamber window carried both the source illumination and collected the reflected beam (after two passes through the sample, integration time 3 ms) to a Zeiss MCS250 Spectrometer (Karl Zeiss, Jena, Germany). Measurements were also made in a simple transmission geometry using a modified chamber with a second glass window beneath the sample on a glass substrate.

Supporting Information

Supporting Information is available from the Wiley Online Library or from the author.

Acknowledgements

The authors thank Dr. Sven Hüttner for help with ellipsometry measurements, Dr. Barbara Heck for GIWAXS, and Dr. Martin

Brinkmann for TEM measurements and for valuable discussions. This work was funded by the Freiburg Institute for Advanced Studies. S.L. thanks the Landesstiftung Baden-Wuerttemberg and the DFG for a grant within the Emmy Noether Program and the priority program SPP1355. U.S. acknowledges funding from EPSRC (EP/F056702/1).

Received: August 16, 2010

---

[1] H. Sirringhaus, P. J. Brown, R. H. Friend, M. M. Nielsen, K. Bechgaard, B. M. W. Langeveld-Voss, A. J. H. Spiering, R. A. J. Janssen, E. W. Meijer, P. Herwig, D. M. de Leeuw, *Nature* **1999**, *401*, 685.
[2] J. Lim, S. Ferdous, M. Muthukumar, A. Briseno, *Mater. Today* **2010**, *13*, 14.
[3] Y. Lan, C. Yang, H. Yang, *Polym. Int.* **2010**, *59*, 16.
[4] R. A. Street, *Nature* **2006**, *5*, 171.
[5] J. Chang, B. Sun, D. W. Breiby, M. M. Nielsen, T. I. Sölling, M. Giles, I. McCullough, H. Sirringhaus, *Chem. Mater.* **2004**, *16*, 4772.
[6] H. Yang, T. J. Shin, L. Yang, C. Y. Ryu, Z. Bao, *Adv. Funct. Mater.* **2005**, *15*, 671.
[7] H. Yang, S. W. LeFevre, C. Y. Ryu, *Appl. Phys. Lett.* **2007**, *90*, 172116.
[8] J. Chang, J. Clark, N. Zhao, H. Sirringhaus, D. Breiby, J. W. Andreason, M. M. Nielsen, M. Giles, M. Heeney, I. McCullough, *Phys. Rev. B* **2006**, *74*, 115318.
[9] S. Joshi, P. Pingel, S. Grigorian, T. Panzner, U. Pietsch, D. Neher, M. Forster, U. Scherf, *Macromolecules* **2009**, *42*, 4651.
[10] L. H. Jimison, M. F. Toney, I. McCulloch, M. Heeney, A. Salleo, *Adv. Mater.* **2009**, *21*, 1.
[11] M. Brinkmann, P. Rannou, *Macromolecules* **2009**, *42*, 1125.
[12] P. Pingel, A. Zen, R. D. Abellón, F. C. Grozema, L. D. A. Siebbeles, D. Neher, *Adv. Funct. Mater.* **2010**, *20*, 2286.
[13] R. Kline, M. McGehee, E. Kadnikova, J. Liu, J. Frechet, M. Toney, *Macromolecules* **2005**, *38*, 3312.
[14] A. Zen, M. Saphiannikova, D. Neher, J. Grenzer, S. Grigorian, U. Pietsch, U. Asawapirom, S. Janietz, U. Scherf, I. Lieberwirth, G. Wegner, *Macromolecules* **2006**, *39*, 2162.
[15] I. McCullough, M. Heeney, C. Bailey, K. Genevicius, I. Macdonald, M. Shkunov, D. Sparrowe, S. Tierney, R. Wagner, W. Zhang, M. L. Chabinyc, R. J. Kline, M. Mcgehee, M. F. Toney, *Nat. Mater.* **2006**, *5*, 328.
[16] M. Surin, P. Leclère, R. Lazzaroni, J. D. Yuen, G. Wang, D. Moses, A. J. Heeger, S. Cho, K. Lee, *J. Appl. Phys.* **2006**, *100*, 033712.
[17] G. Wang, J. Swensen, D. Moses, A. J. Heeger, *J. Appl. Phys.* **2003**, *93*, 6137.
[18] D. H. Kim, Y. Jang, Y. D. Park, K. Cho, *J. Phys. Chem. B* **2006**, *110*, 15763.
[19] J. Clark, J. Chang, F. C. Spano, F. H. Friend, C. Silva, *App. Phys. Lett.* **2009**, *94*, 163306.
[20] A. J. Kovacs, D. J. Blundell, A. Keller, *Polym. Lett.* **1966**, *4*, 481.
[21] J. Xu, Y. Ma, M. Rehahn, G. Reiter, *Nat. Mater.* **2009**, *8*, 348.
[22] G. Lu, L. Li, X. Yang, *Adv. Mater.* **2007**, *19*, 3594.
[23] G. Lu, L. Li, X. Yang, *Macromolecules* **2008**, *41*, 2062.
[24] J. Clark, C. Silva, R. H. Friend, F. C. Spano, *Phys. Rev. Lett.* **2007**, *98*, 206406.
[25] G. W. Hener, D. S. Pearson, *Macromolecules* **1991**, *24*, 6295.
[26] J. Liu, R. Loewe, R. D. McCullough, *Macromolecules* **1999**, *32*, 5777.